Annu. Rev. Nucl. Part. Sci. 1991. 41: 321–55

SUPERDEFORMED NUCLEI[1]

Robert V. F. Janssens and Teng Lek Khoo

Argonne National Laboratory, Argonne, Illinois 60439

KEY WORDS: superdeformation, high spin states, collective nuclear models

CONTENTS

1. INTRODUCTION

The ever increasing accuracy with which nuclear structure studies can be performed experimentally and theoretically has yielded a wealth of fascinating new results. It is by now well known that throughout the

[1]The US Government has the right to retain a nonexclusive royalty-free license in and to any copyright covering this paper.

periodic table nuclei can adopt a rich variety of shapes, particularly when rotated. The shape changes result from the interplay between macroscopic (liquid-drop) and microscopic (shell-correction) contributions to the total energy of the nucleus. The shell correction is a quantal effect arising from the occupation of nonuniformly distributed energy levels. Rotation affects the nuclear shape by modifying both the liquid-drop moment of inertia and the nucleonic occupation of specific shape-driving orbitals. Many interesting phenomena have been reported in rapidly rotating nuclei; examples are the alignment of particle spins along the rotation axis (backbending), the transition from prolate collective to oblate aligned-particle structures (band termination), the possible occurrence of triaxial shapes, and the onset of octupole instabilities. The most spectacular experimental result to date is the discovery of superdeformation, in which nuclei are trapped in a metastable potential minimum associated with very elongated ellipsoidal shapes corresponding to an axis ratio of roughly 2:1.

Superdeformation was first proposed some twenty years ago to explain the fission isomers observed in some actinide nuclei (1, 2). It was later realized that superdeformed shapes can occur at high angular momentum in lighter nuclei (3–7). The interest in the mechanisms responsible for these exotic shapes has increased enormously with the discovery of a superdeformed band of nineteen discrete lines in ^{152}Dy (8). At about the same time, evidence for highly deformed nuclei (axis ratio 3:2) was also reported near ^{132}Ce (9). Striking properties emerged from the first experiments, such as the essentially constant energy spacing between transitions ("picket-fence" spectra), the unexpectedly strong population of superdeformed bands at high spins, and the apparent lack of a link between the superdeformed states and the yrast levels.

These findings were reviewed by Nolan & Twin (10). The present article follows upon their work and discusses the wealth of information that has since become available. This includes the discovery of a new "island" of superdeformation near $A = 190$, the detailed spectroscopy of "ground" and excited bands in the superdeformed well near $A = 150$ and $A = 190$, the surprising occurrence of superdeformed bands with identical transition energies in nuclei differing by one or two mass units, and the improved understanding of mechanisms responsible for the feeding into and the decay out of the superdeformed states.

2. A NEW REGION OF SUPERDEFORMATION

2.1 *Calculations of Superdeformed Shapes*

As alluded to above, the single-particle energy spectrum plays an essential role in determining the nuclear shape. The stability of spherical nuclei at

closed shells is related to large gaps in the energy level spectrum of the various orbitals. Shell gaps also occur in the single-particle spectrum for specific deformations. In an axially symmetric harmonic oscillator (11), these shell gaps occur when the lengths of the principal axes form integer ratios and, in particular, when the ratio is 2:1:1, which corresponds to a quadrupole deformation β_2 (12) of 0.65. These shell corrections, superimposed on a smooth liquid-drop contribution, can generate local minima in the potential energy surface. The cranked-Strutinsky method is often used to calculate potential energy surfaces. In this approach, the total energy of a nucleus is calculated as a sum of liquid-drop and shell-correction terms. The liquid-drop energy is a sum of Coulomb, surface, and rotational energies. All of these terms are calculated as a function of nuclear deformation. In the heaviest nuclei, strong Coulomb forces favor large deformations, balancing the surface energy (which favors compact shapes). Because of this balancing, shell corrections at large deformations give rise to pronounced potential minima that are responsible for the fission isomers (1). At high spin in the $A = 150$ region, it is the rotational energy term that balances out the surface term at large deformation and makes superdeformation possible. Several cranked-Strutinsky calculations, using either an anharmonic oscillator potential (5, 13) or a Woods-Saxon potential (6, 7), have been quite successful in predicting the existence of an "island" of superdeformation for $Z \approx 64$ and $N \approx 86$ as well as the occurrence of "nearly" superdeformed nuclei ($\beta_2 = 0.4$) for $Z \approx 58$ and $N \approx 74$. The calculations indicate that pronounced secondary minima are obtained only when both proton and neutron shell corrections are favorable and this leads to the occurrence of these "islands" in the periodic table.

Superdeformed minima in a great number of nuclei with $Z \geq 80$ were originally predicted by Tsang & Nilsson (3) at zero spin and later confirmed in several other calculations. From general expectations (e.g. 5), these minima survive and come closer to the yrast line with increasing spin. More recent calculations (13–15) suggest that the superdeformed minimum becomes yrast at spins in excess of $30\hbar$ in nuclei with $Z \approx 80$, $N \approx 112$. Calculated potential energies (15) as a function of quadrupole deformation are presented in Figure 1 for different spin values in the nucleus ^{191}Hg. From the figure, it is clear that a deep minimum exists at very large deformation ($\beta_2 \approx 0.5$, axis ratio ≈ 1.65:1) and this minimum is calculated to persist down to the lowest spins, even though the well depth diminishes. Here, strong Coulomb and rotational effects both play a significant role. The occurrence of a superdeformed minimum at zero spin in the $A = 190$ region has also been predicted in calculations using static, self-consistent Hartree-Fock and Hartree-Fock-Bogoliubov calculations (16, 17).

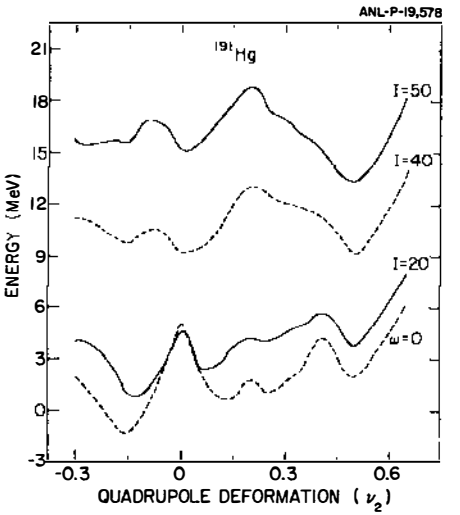

Figure 1 Total energy as a function of quadrupole deformation for different spin values in ^{191}Hg [from (15); ν_2 is related to β_2, $\nu_2 = 0.5$ when $\beta_2 = 0.55$].

2.2 *The First Superdeformed Band in the* A = *190 Region*

Experimental evidence for a new region of superdeformation near $A = 190$ first became available in 1989. As can be seen in Figure 2, a weak rotational band of 12 transitions was observed in the nucleus ^{191}Hg (18). The measured properties of this band identify it as a superdeformed band: (*a*) the average energy spacing is small (37 keV) and corresponds to an average dynamic moment of inertia $J^{(2)}$ of $110\hbar^2$ MeV^{-1}, which agrees well with expectations based on cranked-Strutinsky calculations (15); and (*b*) the measured average quadrupole moment of 18 ± 3 eb implies a large quadrupole deformation ($\beta_2 \approx 0.5$). The band also exhibits other characteristics that are similar to those noted for superdeformed bands in the $A = 150$ region; (*a*) the small total intensity with which the band is fed (the flow through the band represents $\sim$2% of the ^{191}Hg intensity); (*b*) the intensity pattern (which shows the γ-ray intensity in the band decreases gradually with increasing γ-ray energy, while at the bottom of the cascade it remains constant over the last 3–4 transitions); and (*c*) the fact that the transitions linking the superdeformed band to the yrast states could not be observed.

Several important questions were raised by the original experimental result. First, $J^{(2)}$ was found to increase steadily with the rotational frequency $\hbar\omega$ (defined as $E_\gamma/2$). Mean-field calculations that attempt to reproduce variations in $J^{(2)}$ suggest that such a rise may be attributed to three major factors, contributing either separately or cooperatively: (*a*) shape changes as a function of $\hbar\omega$ (e.g. centrifugal stretching), (*b*) changes in

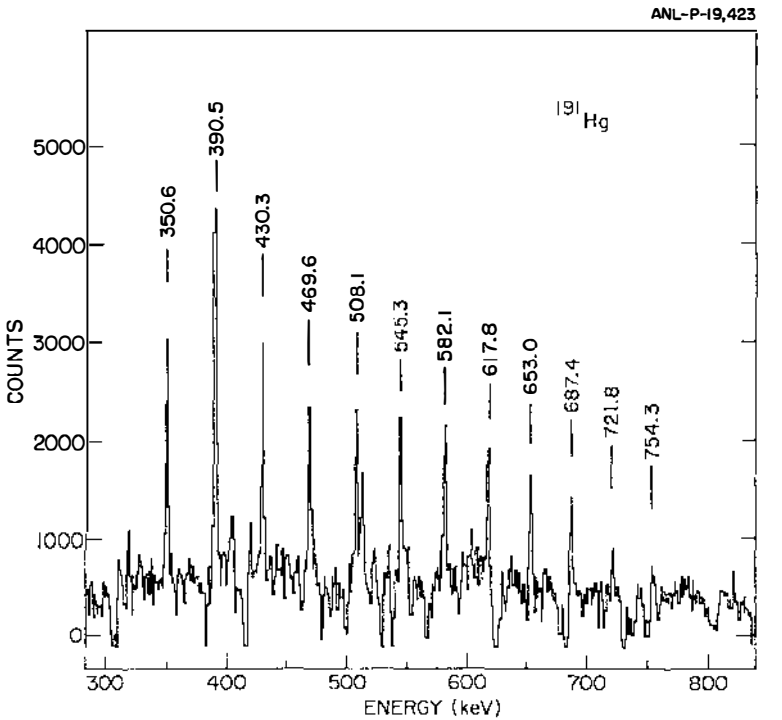

Figure 2 The γ-ray spectrum of the first superdeformed band observed in the $A = 190$ region (18). The 390-keV transition is an unresolved doublet consisting of a transition in the superdeformed band and the $17/2^+$-$13/2^+$ ground-state transition in ^{191}Hg.

pairing at large deformations (19), and (*c*) occupation of specific high-$\mathcal{N}$ orbitals (19,20) (i.e. high-$\mathcal{N}$ orbitals from two major shells higher, which plunge down as a function of deformation and approach the Fermi surface at very large deformations, in this case $i_{13/2}$ protons and $j_{15/2}$ neutrons). Second, this superdeformed band was found to decay only to the $17/2^+$ yrast state of ^{191}Hg. Thus one could neither obtain a firm indication of the spins of the superdeformed states nor assess whether the link between superdeformed states and the yrast levels is statistical in nature, as in the $A = 150$ region (10), or whether it occurs only through a few specific transitions. Finally, questions concerning the existence of other superdeformed nuclei [as predicted by theory (15)] and the limits in N and Z of the superdeformed region also needed attention.

2.3 *Superdeformation in ^{192}Hg*

An impressive number of new results in the $A = 190$ region have become available recently. However, before presenting these we first summarize

the present experimental situation concerning ^{192}Hg, the nucleus regarded as the analogue of ^{152}Dy for this region in the sense that shell gaps are calculated (15, 21) to occur at large deformation for both $Z = 80$ and $N = 112$ (see below). The gamma spectrum of the superdeformed band in ^{192}Hg, measured with the ^{160}Gd(^{36}S,4n) reaction at 162 MeV (22), is presented in Figure 3*a*. [The 16 transitions have also been observed in an independent experiment (23).] The total flow through the band represents 1.9% of all transitions in ^{192}Hg. From Figure 3*a* it is clear that the band feeds the known levels up to 8^+ in the positive-parity yrast sequence and up to 9^- in the negative-parity band. Transitions linking the superdeformed band with known yrast levels could not be found. It is likely that many different decay paths share the intensity and that the link is statistical in nature. This assumption is supported by the observation that the feeding into the yrast states is spread over several states belonging to bands of opposite parity with rather different intrinsic structure (24). Thus, the mechanism of deexcitation out of the superdeformed bands in this region appears to be similar to that discussed for the $A = 150$ region (10).

As with ^{191}Hg, the transition energies in the superdeformed band of ^{192}Hg extend to much lower energy than in superdeformed bands of the $A = 150$ region (the lowest transition energy in ^{152}Dy is 602 keV, as opposed to 257 keV in ^{192}Hg). If transition energies (and rotational frequencies) can be related to spin, this result indicates that superdeformation persists to lower spin in the new region. The data on ^{192}Hg allow for the verification of this assertion. The spin of the lowest level in the superdeformed band was estimated to be $10\hbar$ from the average entry spin ($8\hbar$) into the yrast states (22, 23) and from the assumption of a $\Delta I = 2\hbar$ angular momentum removal by the transitions linking the superdeformed states and the yrast line. The same spin value is also obtained from a procedure in which $\mathcal{J}^{(2)}$ is fit by a power series expansion in ω^2, which is then integrated to give the spin (see Section 4.2) (23). With these assumed spin values, a static moment of inertia $\mathcal{J}^{(1)}$ can be derived: the latter is presented as a function of $\hbar\omega$ together with the values of $\mathcal{J}^{(2)}$ in Figure 3*b*. It is striking that (*a*) there is a large monotonic increase (40%) in $\mathcal{J}^{(2)}$ with $\hbar\omega$; (*b*) the $\mathcal{J}^{(2)}$ values for ^{192}Hg are similar to, but always higher than, those for ^{191}Hg at the same frequency; and (*c*) $\mathcal{J}^{(2)}$ is significantly larger than $\mathcal{J}^{(1)}$ for all values of $\hbar\omega$.

Crucial information regarding the properties of the ^{192}Hg superdeformed band were provided by detailed measurements of lifetimes with the Doppler-shift attenuation method (DSAM) (25). In contrast with previous measurements for superdeformed states, where only fractional Doppler shifts $F(\tau)$ were reported (10, 18), Moore et al analyzed detailed

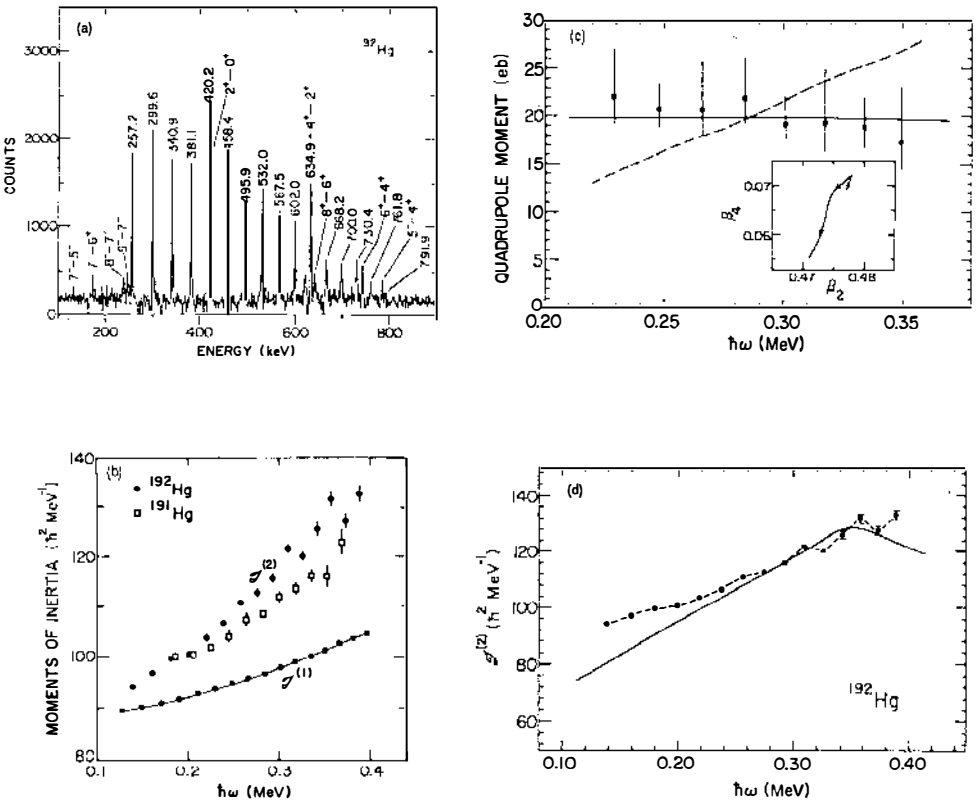

Figure 3 (*a*) Gamma spectrum of the superdeformed band in ^{192}Hg obtained from the sum of selected coincidence spectra (22). The energies of the superdeformed transitions are indicated and transitions between yrast states are also given.

(*b*) Comparison between the dynamic moments of inertia $\mathcal{J}^{(2)}$ for the superdeformed bands in ^{191,192}Hg. The static moment of inertia $\mathcal{J}^{(1)}$ is also given for ^{192}Hg assuming spin values for superdeformed states discussed in the text.

(*c*) Comparison between the measured and calculated transition quadrupole moments Q_t in the superdeformed band of ^{192}Hg (25). The dashed line represents a calculation assuming that the rise in $\mathcal{J}^{(2)}$ is due to centrifugal stretching, the solid line is the result of a cranked shell model calculation discussed in the text, and the inset shows the calculated change in the deformation parameters over the frequency range of interest (the arrows point toward increasing frequency).

(*d*) Comparison between the measured and calculated $\mathcal{J}^{(2)}$ values for the superdeformed band in ^{192}Hg (25).

line shapes for individual transitions between superdeformed states. Such an analysis allows one to determine the variation of transition quadrupole moment (Q_t) as a function of $\hbar\omega$, as opposed to previous studies in which Q_t was assumed to be constant for all states in the band. The measured lifetimes τ were transformed into transition quadrupole moments $Q_t(I) = (1.22\langle I020|I-20\rangle^2\tau E_\gamma^5)^{-1/2}$ assuming the spin values given above. The Q_t values are displayed as a function of $\hbar\omega$ in Figure 3*c*. As can be seen, the quadrupole moment Q_t, and hence the deformation, remain essentially constant ($Q_t \approx 20 \pm 2$ eb) over the entire frequency range. This result rules out centrifugal stretching as an explanation for the rise in $J^{(2)}$: this is illustrated by the dashed line in Figure 3*c*, where the values of Q_t have been derived assuming that the change in $J^{(2)}$ is entirely due to a variation in deformation.

Bengtsson et al have shown that the occupation of specific high-$\mathcal{N}$ intruder orbitals plays an important role in understanding the variations of $J^{(2)}$ with mass number and rotational frequency in the $A = 150$ region (20). This effect alone cannot account for the variation in $J^{(2)}$ in ^{191,192}Hg: mean-field calculations without pairing, such as those by Chasman (15) or Åberg (13), give proton and neutron contributions to $J^{(2)}$ that remain essentially constant with $\hbar\omega$. This finding emphasizes the need to examine the effects of pairing (changes in pairing at large deformations) as first pointed out by Ye et al (22). This is best done in the framework of cranked deformed shell model calculations that include the effects of static and dynamic pairing, using either the Woods-Saxon or the modified-oscillator approach. The basis for these calculations is discussed in detail elsewhere (26, 27) as are the first applications to the Hg nuclei (21, 25, 28, 29).

The neutron and proton Woods-Saxon routhians for large deformation are presented in Figure 4 (21). Notice that the large $Z = 80$ shell gap remains at all rotational frequencies. In the neutron system there are two single-particle gaps at $N = 112$ and $N = 116$, separated by two high-K levels [512]5/2 and [624]9/2. Because of these shell gaps, $^{192}_{80}\mathrm{Hg}_{112}$ can be regarded as a doubly magic nucleus in the superdeformed well. For this nucleus the relevant high-$\mathcal{N}$ intruder orbitals occupied in the superdeformed configuration are four ($i_{13/2}$) protons and four ($j_{15/2}$) neutrons. Adopting the nomenclature of Bengtsson et al (20), we can label the superdeformed configuration in ^{192}Hg as $(\pi 6^4 \nu 7^4)$. Figure 3*d* compares the calculated dynamic moment of inertia with the data. In the calculation, pairing correlations were treated self-consistently by means of the particle number projection procedure (26), but the neutron pairing interaction strength was reduced. The rise in the calculated $J^{(2)}$ can be ascribed to the combined gradual alignment of a pair of $\mathcal{N} = 6$ ($i_{13/2}$) protons and of a pair of $\mathcal{N} = 7$ ($j_{15/2}$) neutrons within the frequency range under con-

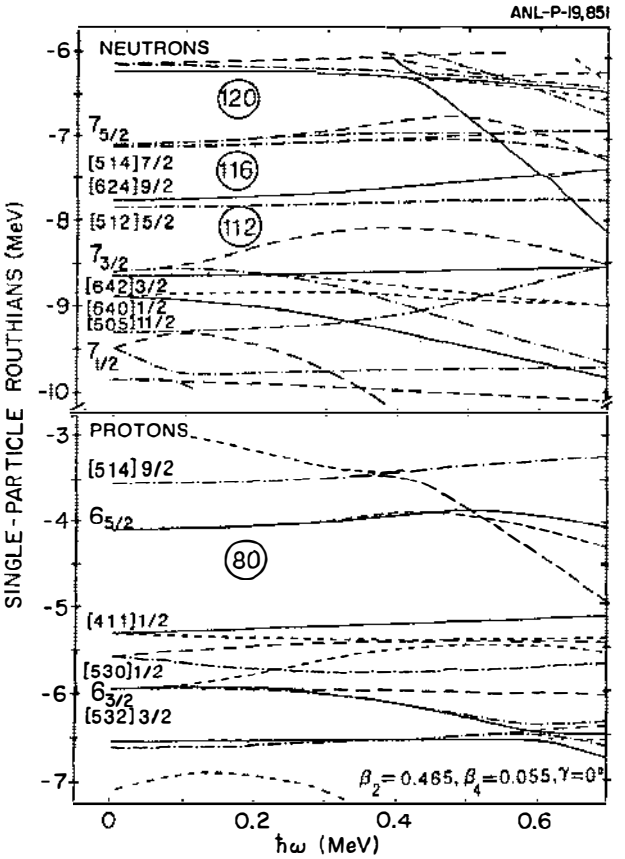

Figure 4 Neutron and proton Woods-Saxon routhians for ^{192}Hg calculated for the deformation parameters β_2, β_4, and γ indicated. The orbitals are labeled by their asymptotic Nilsson quantum numbers $[\mathcal{N}n_3\Lambda]\Omega$ or, in the case of the high-$\mathcal{N}$ intruder orbitals, by $\mathcal{N}_\Omega$. The conventions for labeling the orbitals are from Riley et al (21).

sideration. The data are reproduced rather well. The evolution of the nuclear shape with $\hbar\omega$ was also calculated. The inset in Figure 3*c* illustrates that within the frequency range of interest the predicted changes in the β_2 and β_4 deformation parameters are very small. The resulting Q_t values agree well with the measured values, as is shown by the solid line in Figure 3*c*. The success of the calculations in reproducing all aspects of the data allows one to propose that quasi-particle alignments and the resulting changes in pairing are major contributors to the rise in $J^{(2)}$ in ^{192}Hg

and, probably, in other nuclei in this region. Further evidence for this conclusion, as well as for the power of calculations, is discussed below.

2.4 *Neutron and Proton Excitations in the Superdeformed Minimum*

Figure 5 presents the dynamic moments of inertia of all the superdeformed bands observed so far in the $A = 190$ region: bands have been identified in all Hg isotopes with $A = 189$–194 (18, 21–23, 28, 30–33), in ^{193,194}Tl (34, 35), and in ^{194,196}Pb (36, 37). Furthermore, in many nuclei several superdeformed bands have been reported. Thus, just as in the $A = 150$ region discussed below, it has been possible to perform detailed spectroscopy in the superdeformed well. Most of the data can be understood in the framework of the cranked shell model calculations with pairing (introduced in Section 2.3), and specific configurations have been proposed for many of the bands of Figure 5 (21, 29). Neutron configurations involving the intruder orbital $7_{3/2}$ and/or the [642]3/2, [512]5/2, and [624]9/2 levels (Figure 4) have been proposed for the superdeformed bands in the Hg isotopes (the proton configuration is always $\pi 6^4$). In ^{194}Hg, for example, the superdeformed yrast band still contains the $\pi 6^4 \nu 7^4$ configuration, but the lowest neutron excitations are predicted to involve promotion from the [512]5/2 to the [624]9/2 levels. This leads to two pairs of strongly coupled bands with negative parity showing no signature splitting. Three superdeformed bands have been observed in this nucleus (21, 33). Their properties match the expectations: the two excited bands are interpreted as one signature partner pair, since the γ-ray energies in one of the bands are observed to lie midway between those of the other within 1 keV over the entire frequency range, and both bands are of similar intensity. Equally successful comparisons between the data and the calculations can be made for the bands of the other Hg isotopes. The only notable exception is ^{193}Hg, where some of the observed features, such as the irregularities in the evolution of $J^{(2)}$ with $\hbar\omega$ for two of the bands (Figure 5), cannot be readily understood within the framework of the calculations (32). The suggestion has been made that octupole effects must be taken into account. This is discussed in Section 5.

The cranked shell model calculations with pairing appear to be equally successful in describing proton excitations. Considering the proton routhians of Figure 4, the [411]1/2, [530]1/2, and [532]3/2 levels are important for superdeformed nuclei with $Z \leq 80$, while the third $i_{13/2}$ ($6_{5/2}$ in Figure 4) intruder orbital and the [514]9/2 state should characterize superdeformed bands in the Tl and Pb nuclei. No superdeformed bands have yet been observed in Au or Pt nuclei, which may underline the importance of the $Z = 80$ shell gap. On the other hand, superdeformed bands have been

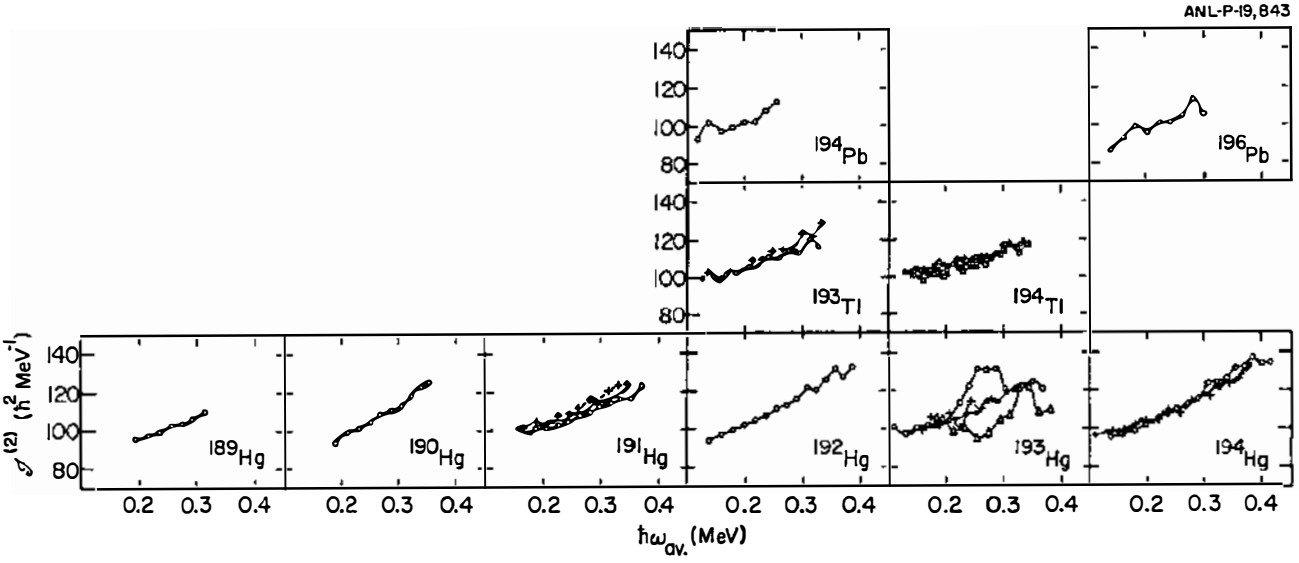

Figure 5 Dynamic moments of inertia $J^{(2)}$ as a function of rotational frequency for all superdeformed bands in the $A = 190$ region. The data are from (18, 21–23, 28, 30–37).

seen in several Pb and Tl nuclei (34–37). In ^{193}Tl, for example, the yrast superdeformed configuration is labeled as $\pi 6^5$ in the calculations, and it exhibits some signature splitting at $\hbar\omega \geq 0.2$ MeV (Figure 4). Thus one would expect to observe two signature partner bands, and indeed they were seen experimentally (34).

A direct comparison of the $\mathcal{J}^{(2)}$ values for ^{193}Tl with those observed in ^{192}Hg and in the first ^{191}Hg superdeformed band (which, as ^{193}Tl, is thought to contain a single nucleon in a high-$\mathcal{N}$ intruder orbital) is also particularly revealing (Figure 6). The occupation of the third $i_{13/2}$ orbital in ^{193}Tl increases the value of $\mathcal{J}^{(2)}$ with respect to ^{192}Hg at the lowest frequencies. In both ^{191}Hg and ^{193}Tl, $\mathcal{J}^{(2)}$ is essentially constant at the lowest frequencies before it exhibits the characteristic rise described above. This feature is also present in the calculations and is proposed to be a signature for the occupation of these high-j intruder orbitals by a single nucleon (34). In the ^{191}Hg band, the alignment of the $j_{15/2}$ neutron is blocked, and the rise in $\mathcal{J}^{(2)}$ is attributed to the alignment of the $i_{13/2}$ protons; in ^{193}Tl the opposite situation occurs. The fact that the rise in $\mathcal{J}^{(2)}$ with $\hbar\omega$ is very similar in both cases implies that neutron and proton alignments make contributions of comparable magnitude. Furthermore, the rise of $\mathcal{J}^{(2)}$ in ^{193}Tl starts at lower frequency that that in ^{191}Hg. This suggests that the neutrons align at somewhat lower frequency than the protons, in agreement with the calculations.

From the discussion above, it can be concluded that a good description

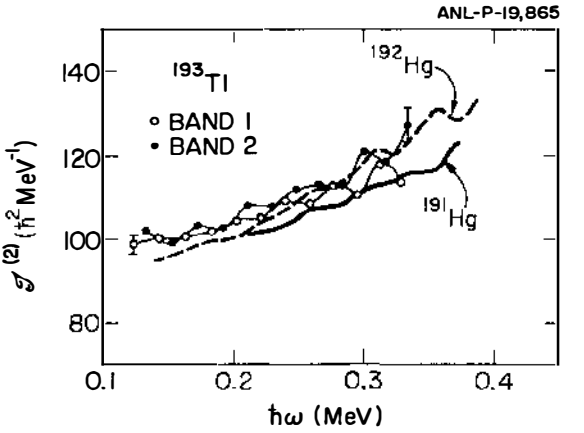

Figure 6 Comparison between the dynamic moments of inertia $\mathcal{J}^{(2)}$ measured in the superdeformed bands of ^{193}Tl, ^{192}Hg, and ^{191}Hg (yrast superdeformed band). The data are from (22, 28, 34).

of the superdeformed bands within the framework of cranked shell model calculations with pairing can be achieved. Two points need to be emphasized, however. First, the transition energies in some of the superdeformed bands are surprisingly close to those of bands in neighboring nuclei and several bands can be related to ^{192}Hg (40). This property is discussed in Section 4. Second, the inclusion of pairing is crucial for reproducing the data and, in particular, the smooth increase of $\mathcal{J}^{(2)}$ with $\hbar\omega$. In the proton system, pairing is reduced by the presence of the $Z = 80$ shell closure. As was shown by Riley et al (21) and by Carpenter et al (28), the calculations require that the neutron pairing be reduced as well if one wants to reproduce the similarities in the behavior of $\mathcal{J}^{(2)}$ with $\hbar\omega$ observed in *all* nuclei in this region.

Reduced pairing is to be expected on the basis of general arguments (38). Pairing is sensitive to the overlap between orbitals of interest. At the very large deformations being considered here, states originating from different shells approach the Fermi level, and these states will only be very weakly coupled through the pairing interaction. Moreover, the coupling between the all-important unique-parity levels (that is, the various components of the high-$\mathcal{N}$ intruders) is also severely reduced because of their sizable energy splitting at large deformation. First attempts to provide a quantitative estimate of the reduction in pairing have recently been made (38, 39).

3. SUPERDEFORMATION IN THE $A = 150$ REGION: "IDENTICAL" BANDS

3.1 *High-$\mathcal{N}$ Orbital Assignments in the Superdeformed Minimum*

Since the review by Nolan & Twin (10) discussing the two first superdeformed bands of the $A = 150$ region (^{152}Dy and ^{149}Gd), the "island" of superdeformed nuclei in this mass region has expanded considerably. Superdeformed bands have now been identified in all Gd isotopes with $A = 146$–150 (41–46), in ^{150,151}Tb (44, 45, 47), and in $^{151-153}$Dy (8, 48, 49). Furthermore, in many cases several superdeformed bands have been seen in the same nucleus: a summary of the available data on the $\mathcal{J}^{(2)}$ moments of inertia is presented in Figure 7. Preliminary reports of similar band structures in ^{145}Gd and ^{142}Eu have also become available (50, 51). As in the $A = 190$ region, differences in the variations of $\mathcal{J}^{(2)}$ with $\hbar\omega$ from nucleus to nucleus have been attributed to the occupation of specific high-$\mathcal{N}$ intruder orbitals. In the $A = 150$ region, $^{152}_{66}\mathrm{Dy}_{86}$ can be described as the "doubly magic" nucleus: all available calculations indicate the presence

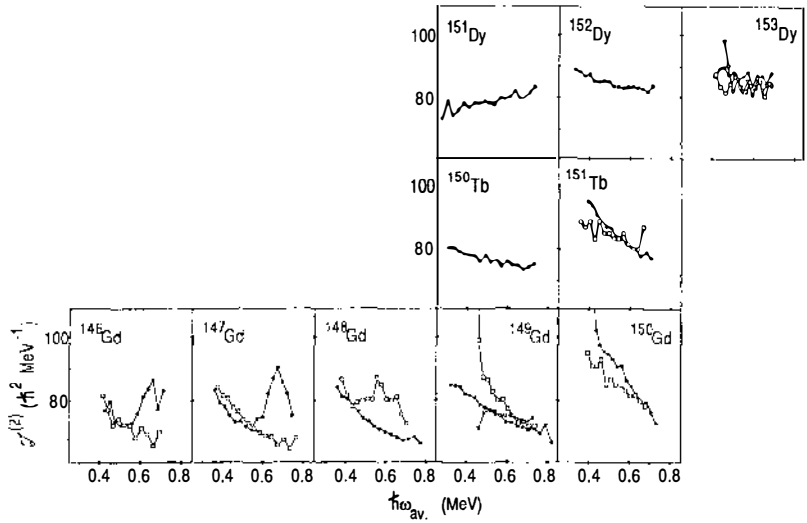

Figure 7 Dynamic moments of inertia $J^{(2)}$ for all superdeformed bands in the $A = 150$ region. The data are from (8, 10, 41–49).

of very large shell gaps at $Z = 66$ and $N = 86$ for a quadrupole deformation $\beta_2 \approx 0.6$.

The occupation of specific high-$\mathcal{N}$ intruder orbitals can have dramatic effects: in the Dy isotopes for example, $J^{(2)}$ rises smoothly over the entire frequency range in ^{151}Dy (Figure 7), while a smooth decrease is seen in ^{152}Dy and an essentially constant value of $J^{(2)}$ is observed for the yrast superdeformed band in ^{153}Dy (it is assumed that the most intensely populated band is the "ground" band in the second well). For these isotopes, the proton contribution has been assigned as $\pi 6^4$ (i.e. $i_{13/2}$) and the observed differences have been attributed to changes in the occupation of the $j_{15/2}$ neutron orbitals ($\nu 7^1$, $\nu 7^2$, and $\nu 7^3$ for $^{151-153}$Dy, respectively), which result in contributions of varying magnitude to $J^{(2)}$ (20). While the calculations of Bengtsson et al (20) were performed without pairing and at a fixed deformation, more recent Woods-Saxon cranked shell model calculations take into account small variations of the shape with spin as well as changes in deformation from one nucleus to another (19, 26). These calculations also treat pairing correlations self-consistently (see also 52).

The best indication for the importance of including pairing correlations and shape effects in this mass region comes from the data on the Gd isotopes. In the yrast superdeformed band of ^{150}Gd, for example, $J^{(2)}$ not only decreases with $\hbar\omega$, but also falls off dramatically at the lowest

frequencies (Figure 7). In the calculations, this band is assigned a $\pi 6^2 \nu 7^2$ configuration. This is in agreement with the assignment made by Bengtsson et al (20), but the alignment of a pair of $j_{15/2}$ neutrons at $\hbar\omega \approx 0.4$ MeV (i.e. a band crossing) has to be invoked to account for the sharp drop in $\mathcal{J}^{(2)}$. The observation that the deexcitation out of the superdeformed band in ^{150}Gd is extremely abrupt, with essentially all the intensity being lost over a single transition, has been interpreted as additional evidence for this band crossing, which in turn requires the presence of the pairing correlations (45). Marked irregularities in the behavior of $\mathcal{J}^{(2)}$ can also be seen in the yrast superdeformed bands of ^{146,147}Gd as well as in an excited band in ^{145}Gd (Figure 7). At present, there is some argument regarding the exact orbitals involved in these crossings as well as concerning the role of pairing and/or octupole correlations (26, 41, 42, 46). The general conclusion, however, remains that in all yrast superdeformed bands near $A = 150$ the variations of $\mathcal{J}^{(2)}$ with $\hbar\omega$ reflect the major role played by the few nucleons in high-$\mathcal{N}$ orbitals, and the adopted configurations are $\pi 6^{2,3,4}$ for Gd, Tb, and Dy respectively; $\nu 7^0$ or $\nu 7^1$ for $N = 82$–85; $\nu 7^2$ for $N = 86$, and $\nu 7^3$ for $N = 87$. The number of occupied intruder orbitals varies in some of the excited bands.

3.2 *Superdeformed Bands with Identical Energies*

The discovery of multiple superdeformed bands within a single nucleus has made it possible to investigate the microscopic structure of both the ground and excited states in the second well. However, a greater impetus for detailed studies of excited bands has been the unexpected discovery that several pairs of related bands have almost identical transition energies. The first reported cases consisted of the pairs (^{151}Tb*, ^{152}Dy) and (^{150}Gd*, ^{151}Tb)—the asterisk denotes an excited superdeformed band—where transition energies in the pair were found to be equal to within 1–3 keV over a span of 14 transitions (53). Later, another similar pair (^{149}Gd*, ^{150}Tb) was found by Haas et al (44) (they used the notation ^{149}Gd** because they suggested that the second excited superdeformed band in ^{149}Gd is involved). This is illustrated in Figure 8, where the difference between "identical" transition energies ΔE_γ is plotted versus the transition energy. On average, the deviation is less than 1 keV for the first pair and only slightly larger for the other two. This implies that transition energies are equal to better than 3 parts in 1000. This is a rather surprising equality and is quite unprecedented in nuclear physics! The γ-ray energies should scale with the moment of inertia $\mathcal{J}$, which is proportional to $A^{5/3}$ ($\mathcal{J} \approx MR^2$); hence, the energies of adjacent mass nuclei would differ by $\sim$14 keV. Furthermore, the spins of corresponding transitions in each pair necessarily differ by $1/2\hbar$, leading to differences in E_γ of $\sim$13 keV.

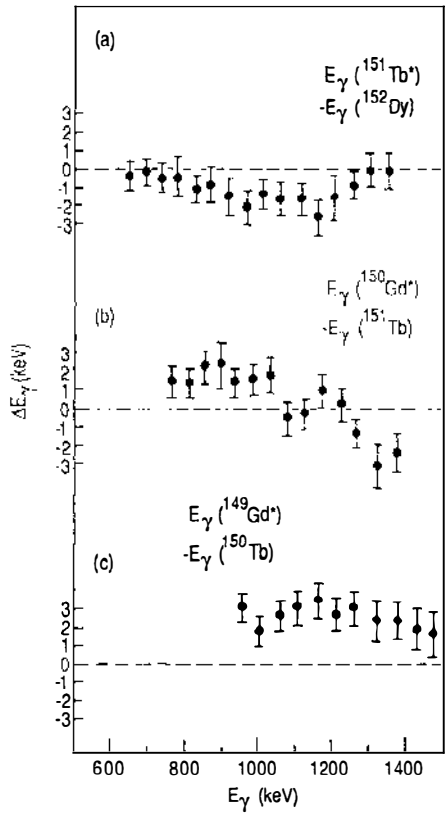

Figure 8 Differences in the γ-ray energies ΔE_γ between the superdeformed bands in (*a*) (^{151}Tb*, ^{152}Dy), (*b*) (^{150}Gd*, ^{151}Tb), and (*c*) (^{149}Gd*, ^{150}Tb). The data are from (44, 53).

For $(A-1^*, A)$ pairs, with A even, these differences would reinforce each other.

A word of caution is in order since it is assumed that each pair of transitions being compared has the appropriate spins $(I+1/2, I)$, but the spins of the superdeformed bands have not been measured. Since the spacing between consecutive transitions in each band is ~ 50 keV, the maximum difference in energy in a pair of bands is ~ 25 keV if no spin correlation is involved. However, with three cases and not just an isolated one, it is unlikely that these degeneracies are accidental. Furthermore, in all three cases the excited $(A-1)^*$ superdeformed band is proposed to be characterized by a hole in the same specific orbital (see below).

A related case of identical transition energies occurs in ^{153}Dy—the first

case in which excited superdeformed bands were reported (49). Here, two excited bands have been interpreted as signature partners, and the averages of the transition energies in the partners reproduce the γ-ray energies in ^{152}Dy within 1–3 keV. Finally, the two superdeformed bands of ^{147}Gd have been related to the yrast superdeformed bands of ^{146}Gd and ^{148}Gd respectively, although the average ΔE_γ values are somewhat larger in this case ($\sim$5 keV) (42). In ^{147}Gd, another relation applies as well: one of the bands has γ-ray energies following closely (1–4 keV) the average of two successive transition energies in ^{148}Gd, while the other band shows the same property when compared with the superdeformed band of ^{146}Gd.

3.3 *Strong Coupling and Identical Bands*

The first attempt at an explanation of this surprising phenomenon was presented by Nazarewicz et al (38, 54). The interpretation is done within the framework of the strong coupling limit of the particle-rotor model, in which one or more particles are coupled to a rotating deformed core and follow the rotation adiabatically. We note that for rotors the γ-ray energy for an $I \rightarrow I-2$ transition is given by

$$E_\gamma = \frac{\hbar^2}{2J}(4I-2). \qquad 1.$$

If the Coriolis force causes alignment i of the particle along the rotation vector $\mathbf{R}$, giving $R = I-i$, then

$$E_\gamma = \frac{\hbar^2}{2J}[4(I-i)-2]. \qquad 2.$$

Equation 2 shows that odd and even nuclei can have identical transition energies if $i = 1/2$, when $J^{\text{odd}} = J^{\text{even}}$. In the strong coupling limit, no alignment is present, i.e. $i = 0$, and the transition energies in an odd nucleus, relative to those in an even-even core, obey simple relations, which are shown in Figure 9 (11). Here the moments of inertia for all cases are assumed to be identical. When $K \neq 1/2$, one can see (Figure 9*a–c*) that

$$1/2[E_\gamma(R+1/2)+E_\gamma(R-1/2)]_{\text{odd}} = E_\gamma(R)_{\text{even}}.$$

This strong coupling relation provides a straightforward explanation for the (^{153}Dy*, ^{152}Dy) pair. The two excited bands in ^{153}Dy have been interpreted as a ^{152}Dy $\otimes$ ν[514]9/2 structure with no signature splitting (26, 49)—the relevant single-particle levels for protons and neutrons at large deformation are presented in Figure 3 of the article by Twin (55).

For a $K = 1/2$ band, the transition energies in the odd nucleus are affected by the decoupling parameter, a, and obey the relation

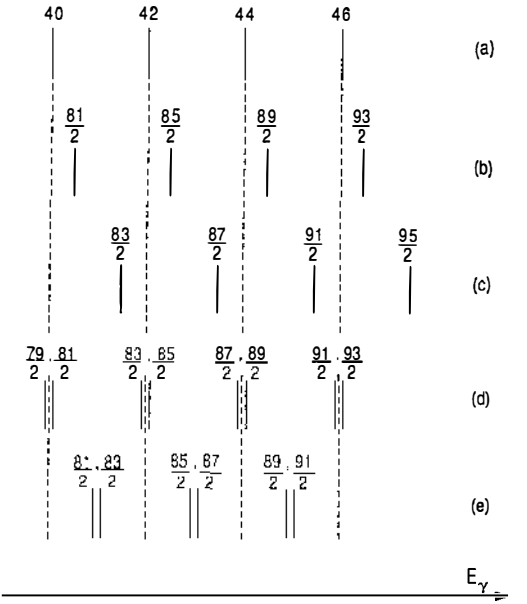

Figure 9 The γ-ray energies for transitions in a perfect rotor, assuming identical moments of inertia in all cases: (*a*) even core; (*b*) and (*c*) odd-even nucleus in the strong coupling limit; (*d*) and (*e*) odd nucleus with $K = 1/2$, $a = +1$, and $a = -1$, respectively. Note that (*d*) and (*e*) also apply for an odd nucleus with alignment $\pm 1/2$, i.e. $I = R \pm 1/2$.

$$E_\gamma = \frac{\hbar^2}{2J}[4I - 2 + 2(-1)^{I+1/2} a \delta_{K,1/2}].$$

The transition energies for $a = \pm 1$ are indicated in Figure 9*d*, *e*. Transitions from both signatures form degenerate doublets, with the $a = 1$ case giving energies identical to those of the core, while the $a = -1$ case has energies midway between those of adjacent transitions in the core. The alignment in a $K = 1/2$ band is given by $i = (-)^{I-1/2} \cdot a/2$.

The three pairs $(A-1^*, A)$ that have identical energies can be interpreted as having $a = 1$. In each case, the $(A-1)^*$ configuration is $A \otimes \pi([301]1/2)^{-1}$. If the decoupling parameter a is calculated from the Nilsson wave function of the [301]1/2 orbital, a value of 0.85 is obtained, very close to but not exactly unity (54). On the other hand, for a $[\mathcal{N} n_3 \Lambda]\Omega$ orbital, the decoupling parameter can be calculated from the asymptotic quantum numbers, by

$$a = (-)^{\mathcal{N}} \delta_{\Lambda,0},$$

which would result in $a = 0$ for the [301]1/2 orbital. However, if one

employed a different coupling scheme in terms of pseudo-spin (see below), the appropriate quantum numbers are $\widetilde{[200]}1/2$, and

$$a = (-)^{\tilde{\mathcal{N}}}\delta_{\tilde{\Lambda},0} = 1,$$

providing a natural explanation for the identical energies of the three pairs. A case where $a = -1$ has not been seen so far, although it is predicted within the pseudo-spin scheme to apply to an excited superdeformed band in ^{151}Dy (38, 54).

It must be stressed again that the explanation of identical energies presented here follows only if the moments of inertia for odd and even nuclei are identical. $A^{5/3}$ scaling would give differences of $\sim 1\%$, as mentioned above. Thus, it still is a puzzle why the moments of inertia J for adjacent nuclei appear to be constant to within $\sim 0.2\%$.

3.4 *Pseudo-spin in Rotating Deformed Nuclei*

A simplified analysis of nucleonic motion and of the effect of deformation can be made within the framework of the pseudo-spin scheme (56–59). In heavy nuclei, this formalism is based on the fact that a major shell, labeled by the total quantum number $\mathcal{N}$, consists of the members of an oscillator shell modified by the removal of the state with largest j $(= \mathcal{N}+1/2)$ and the addition of an intruder orbital with opposite parity and $j = \mathcal{N}+3/2$. The remaining normal-parity orbitals form close-lying doublets with quantum numbers l_1, $j_1 = l_1+1/2$ and $l_2 = l_1+2$, $j_2 = l_2-1/2 = j_1+1$. Examples are the $(d_{5/2}, g_{7/2})$ and $(f_{7/2}, h_{9/2})$ doublets. The doublets can be relabeled in terms of pseudo-quantum numbers $\tilde{l} = l_1+1$, $\tilde{\mathcal{N}} = \mathcal{N}-1$. Thus, the doublets $(d_{5/2}, g_{7/2})$ and $(f_{7/2}, h_{9/2})$ become $\tilde{f}$ and $\tilde{g}$, respectively. A deformed potential preserves this degeneracy: in a Nilsson diagram, close-lying nearly parallel orbits are observed as function of deformation [see, for example, Figure 1 in the article by Bohr et al (59)]. The pair of orbits

$$[\mathcal{N}n_3\Lambda, \Omega = \Lambda+1/2] \quad \text{and} \quad [\mathcal{N}n_3\Lambda+2, \Omega = \Lambda+3/2]$$

can be relabeled with pseudo-quantum numbers

$$[\tilde{\mathcal{N}} = \mathcal{N}-1, n_3, \tilde{\Lambda} = \Lambda+1, \Omega = \tilde{\Lambda}\pm 1/2].$$

The doublet can be viewed as pseudo-spin-orbit partners. The important feature is that the $\tilde{l}\cdot\tilde{s}$ interaction is substantially smaller than the normal $l\cdot s$ coupling. Since the $\tilde{l}\cdot\tilde{s}$ coupling is weak, the Coriolis force readily causes $\tilde{s}$ to align along the rotation vector, i.e. $\tilde{s}_1 = \pm 1/2$. One sees, therefore, that pseudo-spin can lead to $i = 1/2$ in Equation 2 and account for identical transition energies in odd and even nuclei by offsetting the intrinsic spin difference of $1/2\hbar$ (60).

The case for $K = 1/2$ bands has been discussed above, where it was pointed out that the pseudo-spin formalism naturally provides the correct decoupling parameter for explaining bands with identical transition energies. For orbits with $K \neq 1/2$, the alignment in an odd nucleus relative to an even core will, in general, have nonzero contributions from alignment $\tilde{I}_1$ of the pseudo-orbital angular momentum (59). (Only if $\tilde{I}_1 = 0$ will one obtain the simple spectrum given in Figure 9*d*, *e*.) Thus, it will not be easy to find experimental evidence for pseudo-spin alignment by comparing data in odd and even nuclei for orbits with $K \neq 1/2$. However, Hamamoto has suggested that evidence for pseudo-spin alignment may be found in an alignment difference of $1\hbar$ for pairs of orbits that constitute doublets with identical $\tilde{I}_1$ and $\tilde{s}_1 = \pm 1/2$ (I. Hamamoto, private communication) [see also Figures 3 and 4 in the paper by Bohr et al (59)]. Examples of such doublets have so far not been identified. Detection of those doublets will probably require detection of more (weak) excited superdeformed bands, as well as firm spin assignments.

3.5 *Identical Moments of Inertia*

The identical bands discussed above require moments of inertia J in different nuclei to be equal to a remarkable degree. Since J depends on several factors (mass, deformation, polarization effects, alignment, and pairing) the equality in J is very striking and leads one to wonder about the possibility of a fundamental explanation. The standard models are unable to reproduce transition energies with an accuracy of ~ 1 keV. We note that only a few identical bands are observed among the many superdeformed bands in this region and that three of these pairs of bands involve a common orbital. This suggests that the phenomenon is associated with only a few specific orbitals. Indeed, it is recognized that occupation of different high-$\mathcal{N}$ intruder orbits will not result in identical bands because the orbital energies tend to have steep slopes as a function of both deformation and rotational frequency, i.e. strong polarization and alignment effects will result. Ragnarsson used a simple harmonic oscillator model to show that for particles or holes in certain orbitals there can be cancellation among the different terms contributing to changes in J (62). He has been able to reproduce the "identical" energies observed in (^{152}Dy, ^{153}Dy*), where the orbital occupied in ^{153}Dy* is either ν[402]5/2 or ν[514]9/2. These orbitals slope upward with increasing β_2—so-called oblate orbitals—so that a particle here would tend to decrease the deformation of the $(A+1)$ nucleus, compensating the increase in J due to the larger mass. Agreement for other cases calculated by Ragnarsson, including that involving the π[301]1/2 hole (responsible for the three pairs of bands with identical energies), is not as satisfactory, which suggests that other effects, such as

changes in pairing, should be included. A further requirement for the orbital is that the alignment be small, a criterion satisfied by the "oblate" orbitals.

4. IDENTICAL BANDS IN THE $A = 190$ REGION

4.1 *Identical Transition Energies and Relation to* ^{192}Hg

There are even more examples of identical superdeformed bands in the $A = 190$ region than in the $A = 150$ region (63, 64). However, two features distinguish the bands in this region from those near $A = 150$: (*a*) many of the bands occur in pairs separated by two mass units, and (*b*) a large number of bands can be related to the superdeformed band in ^{192}Hg, which appears to serve as a doubly magic core. These features are illustrated in Figure 10*a*, which shows the degree of similarity between transition ener-

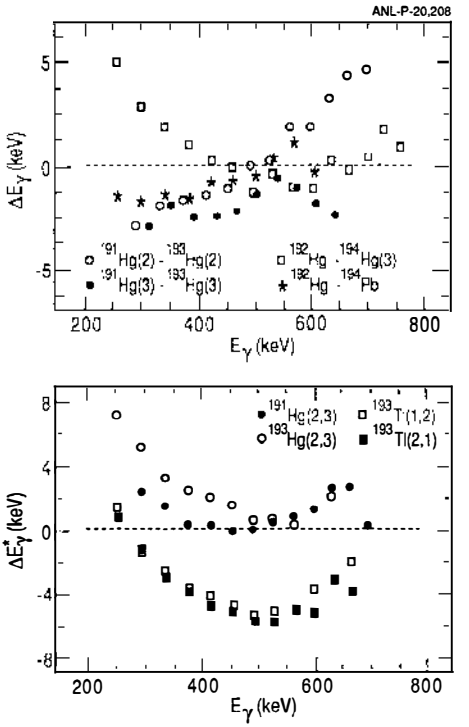

Figure 10 (*a*) Difference in transition energy ΔE_γ, between selected superdeformed bands in the $A = 190$ region.

(*b*) Energy difference ΔE_γ^* (see text) referenced to ^{192}Hg for strongly coupled bands in ^{191,193}Hg and ^{193}Tl. For both (*a*) and (*b*), the data are from (21–23, 28, 34); the figure is adapted from (64).

gies in the pairs [^{191}Hg(2), ^{193}Hg(2)], [^{191}Hg(3), ^{193}Hg(3)], [^{192}Hg, ^{194}Hg(3)], and [^{192}Hg, ^{194}Pb]. (The numbers in parentheses correspond to the labels given to different bands in the original publications; numbers larger than 1 designate excited bands.) Figure 10*b* relates transition energies of ^{192}Hg to those of bands in adjacent nuclei ^{191,193}Hg and ^{193}Tl through the relationship

$$\Delta E_\gamma^* = 1/2\,[E_\gamma^f(R \pm 1/2) + E_\gamma^u(R \mp 1/2)] - E_\gamma^{core}(R),$$

where R is the core angular momentum, and u and f designate transitions from favored and unfavored states in signature partner bands of the odd-even nucleus. As discussed by Satula et al (64) and in Section 2 above, the proposed configurations for these superdeformed bands are characterized by $K \neq 1/2$. As a result both features in Figure 10 can be understood in a straightforward way in the strong coupling scheme, which gives $\Delta E_\gamma^* = 0$. However, there is again the requirement of equal moments of inertia in all nuclei.

Another way of relating the energies of different bands to those of a reference, ^{192}Hg, has been proposed by Stephens et al (40, 63), using the quantity

$$\Delta i = 2\frac{\Delta E_\gamma}{\Delta E_\gamma^{ref}},$$

where $\Delta E_\gamma = E_\gamma - E_\gamma^{ref}$ is obtained by subtracting the transition energy E_γ in a band of interest from the closest transition energy in ^{192}Hg (E_γ^{ref}), and ΔE_γ^{ref} is calculated as the energy difference between the two closest transitions in the reference. Stephens et al called Δi incremental alignment but it is not necessarily related to any physical alignment. In the strong coupling limit, $\Delta i = \pm 1/2$ for an odd nucleus referred to an even core, as can readily be seen in Figure 9*a–c*. For even nuclei, bands with the same or different signatures have $\Delta i = 0$ or 1, respectively. Plots of Δi are shown in Figure 11, which illustrates that the superdeformed bands of the $A = 190$ region can be classified in two families. When additional particles (holes) with respect to ^{192}Hg occupy lower-K members of the high-$\mathcal{N}$ intruder orbitals, values of Δi scatter significantly (Figure 11*a*). This is not surprising since particles in these intruder orbitals tend to both increase deformation and align with rotation, thus making the strong coupling scheme inappropriate. In contrast, when the orbitals involved do not show much variation with $\hbar\omega$ (see Figure 4), that is, when there is little alignment, Δi values fall close to the limits of 0, $\pm 1/2$, ± 1, which are expected in the strong coupling limit (Figure 11*b*).

Stephens et al suggested that many of the cases that exhibit $\Delta i = 0$,

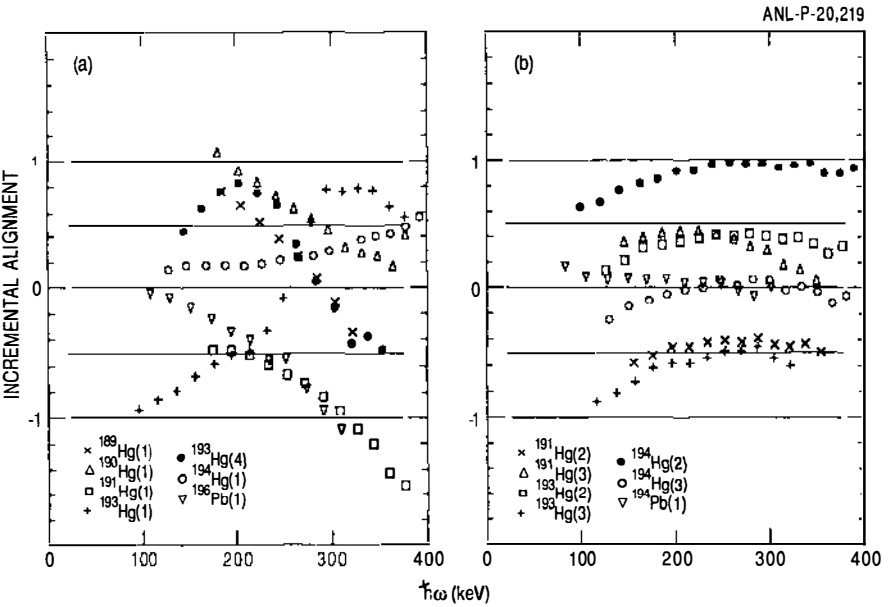

Figure 11 Incremental alignment Δi as a function of rotational frequency for superdeformed bands in $^{189\text{-}194}$Hg (21–23, 28–33) and $^{194\text{-}196}$Pb (36, 37), with ^{192}Hg as a reference. As discussed in the text, the data are divided into two groups in order to illustrate the existence of two families; in (*b*) Δi clusters around integer and half-integer values. The data on superdeformed bands in the Tl isotopes have been omitted for clarity; these are discussed by Azaiez et al (35).

$\pm 1/2$, or ± 1 also have integer alignment differences with respect to the core, which they refer to as quantized alignment (40, 63). While the strong coupling limit corresponds to a zero alignment difference, Stephens et al instead suggest alignments (with respect to ^{192}Hg) of $1\hbar$ in, for example, ^{191}Hg(2,3) and ^{194}Hg(2,3), which are then attributed to pseudo-spin alignment (40). An alignment of $1\hbar$ in ^{191}Hg, instead of the expected $1/2\hbar$, is not easy to understand. However, a word of caution is in order. Whereas extraction of Δi does not require knowledge of spin, determination of alignment does. So far the spins of superdeformed band members have not been assigned using the conventional, tested techniques of γ-ray spectroscopy. Methods to infer the spin have been suggested (23, 65, 66), and are discussed below. At present, it is not established whether these methods give the exact spin or have uncertainties of at least $1\hbar$ (67, 68). Thus, until spins can be assigned firmly, one cannot be certain whether the alignments have the putative value of $1\hbar$ (40) or simply have the value $0\hbar$ expected from strong coupling.

4.2 *Spin Assignments*

Several related procedures for assigning spins to superdeformed states in the $A = 190$ region have been proposed recently (23, 65, 66). These procedures all start from a Harris expansion (69) of the moment of inertia

$$J^{(2)} = J_0 + J_1\omega_x^2 + \cdots$$

and the relation

$$\frac{dI_x}{d\omega_x} = J^{(2)}, \qquad 3.$$

where I_x is the projection of spin along the rotation vector, and $\omega_x = \Delta E_\gamma/\Delta I_x$ is the corresponding rotational frequency. Integrating Equation 3 gives

$$I_x = J_0\omega_x + \frac{J_1}{3}\omega_x^3 + i_0, \qquad 4.$$

where i_0 is the constant of integration. The parameters J_0 and J_1, obtained by fitting $J^{(2)}$ as a function of ω_x, are used to determine I_x with Equation 4. The spin I is then derived from the relation

$$I_x = \sqrt{I(I+1) - K^2},$$

where K is the projection of angular momentum along the symmetry axis. It has been shown that reasonable choices of K do not sensitively affect the derived spin (70). Two assumptions need to be valid for the derived spin to be correct. First, it must be assumed that the fit of $J^{(2)}$ vs ω_x can be correctly extrapolated to zero frequency. [A minimal requirement for this assumption to be correct is that $J^{(2)}$ varies smoothly and gradually in the low frequency domain.] Second, the constant of integration i_0, which corresponds to the alignment at zero frequency must be known. Becker et al (65) and Draper et al (66) assumed that $i_0 = 0$, since this results in calculated values of I that are within $0.1\hbar$ of the integer or half-integer value appropriate for an even or odd nucleus. However, it has not been unambiguously demonstrated that both assumptions are valid. In fact, pairing may well change as $\hbar\omega$ approaches zero, which would lead to uncertainty in the extrapolation of $J^{(2)}$ and result in an "effective" alignment (i.e. an effect that mimics alignment). The extent to which these effects are subsumed into the parameters J_0 and J_1 is not clear. Other attempts at spin determination have concluded that spin uncertainties of at least $1\hbar$ exist (67, 68). Thus, there is a clear need to determine the actual

spins of superdeformed band members experimentally in order to resolve these uncertainties.

4.3 *Strong Coupling Limit and Identical Moments of Inertia*

The discussion above suggested that the identical bands can be understood in terms of the strong coupling limit of the particle-rotor model, with the additional requirement that the moments of inertia be identical. The following questions must then be raised: why does this strong coupling limit work so well and why are the moments of inertia so close? These are interesting questions for theory to address quantitatively, but qualitative comments can be made at this point. As discussed in Section 3.3, the strong coupling limit applies when the alignment is zero. (Assuming equal J values for the bands, the identical energies suggest $i \leq 0.1\hbar$.) At the large deformations discussed here, alignment effects are expected to be small: the large value of the moments of inertia and the increased separation between Nilsson levels from a given shell both reduce the Coriolis coupling responsible for the alignment. In addition, the reduced pairing discussed in Section 2 also leads to less alignment. These qualitative arguments, however, do not guarantee that $i \leq 0.1\hbar$—as implied by the equal transition energies—and, indeed, cranked shell model calculations suggest that alignments of the order of ~ 0.5–$1\hbar$ are obtained (70).

It has been emphasized above that identical transition energies require equal moments of inertia in the bands. This feature is unexpected since the masses involved differ by as much as two units. In the $A = 190$ region, scaling by $J \approx A^{5/3}$ results in a difference of ~ 5 keV per mass unit. Furthermore, bands are compared where the number of quasiparticles associated with the superdeformed configurations differ by one or two. These bands can be expected to have different moments of inertia J because blocking may be present, which would reduce pairing. A major question remains whether the equality of the moments of inertia reflects some hitherto undiscovered symmetry.

Another interesting observation can be added. When $J^{(2)}$ values for all the known superdeformed bands in the $A = 190$ region are compared (see Figure 5), they are all found to cluster within $\lesssim 10\%$ (with the exception of four cases). This is indeed a surprise since bands that differ by 0, 1, or 2 quasiparticle excitations are included. For rotational bands at normal deformation, $J^{(2)}$ values increase by $\sim 15\%$ per quasiparticle because of reduced pairing due to blocking. One wonders if the reduced pairing in superdeformed bands, which is partially responsible for smaller alignment, is also responsible for the noted clustering in $J^{(2)}$ values.

5. OTHER IMPORTANT EFFECTS AT LARGE DEFORMATION

Some pairs of orbitals such as the $i_{13/2}$-$f_{7/2}$ and the $j_{15/2}$-$g_{9/2}$ orbitals that are responsible for strong octupole correlations in light actinide nuclei (71) also appear close to the Fermi level in superdeformed configurations around ^{152}Dy and ^{192}Hg. Several recent calculations indicate that for many superdeformed nuclei the minima in the total energy surfaces exhibit considerable octupole softness, which is expected to persist even at the highest spins (32, 72–75). As a result, collective octupole vibrational excitations can be mixed with low-lying one- and two-quasiparticle states and the excitation pattern near the superdeformed yrast line can be different from that expected for axial symmetry. The calculations suggest that the first excited state in the doubly magic superdeformed nuclei ^{152}Dy and ^{192}Hg should be of collective octupole character and an analogy can be drawn with the well-known collective 3^- state in the doubly magic spherical nucleus ^{208}Pb. Octupole correlations are also expected to reduce single-particle alignments, increase band interactions, and modify the de-excitation pattern of the superdeformed states because of enhanced B(El) rates (71).

Most of the anticipated effects still remain to be observed experimentally. However, first evidence for strong mixing of quasiparticle excitations with octupole vibrations may have been seen in ^{193}Hg (32). In this nucleus, two of the four superdeformed bands are characterized by moments of inertia $J^{(2)}$ strikingly different from those of all other superdeformed bands in this region (see Figure 5), i.e. one shows a strong upbend at the frequency where the other shows a strong downbend. Furthermore, there is indirect experimental evidence for enhanced El transitions linking one of the irregular bands with the yrast superdeformed band. These observations, together with the reduced alignments observed and the strong interaction between the crossing bands, have been interpreted as evidence for strong octupole correlations (32). In the mass $A = 150$ region, one of the proposed explanations for the behavior of one of the superdeformed bands in ^{147}Gd invokes collective octupole excitations as well (42, 76), but other interpretations are also possible (46).

The residual n-p interaction may also play a role in superdeformed nuclei (77). Such an interaction is expected to be strong when protons and neutrons occupy rotationally aligned high-$\mathcal{N}$ intruder orbitals with large spatial overlap, such as the $\pi i_{13/2}$ and $\nu j_{15/2}$ orbitals involved in the superdeformed bands of the $A = 150$ and 190 regions. Such an interaction is expected to lower the energy of superdeformed bands based on these specific intruder configurations with respect to other excitations in the

superdeformed well (77). Firm experimental evidence for the importance of this interaction is currently lacking even though it has been invoked to explain the strong feeding of a superdeformed band in ^{142}Eu (51) (interaction between $\mathcal{N} = 6$ odd proton and odd neutron) and the smooth rise of $J^{(2)}$ with $\hbar\omega$ in the lighter Hg isotopes (interaction between four $\mathcal{N} = 6$ protons and four $\mathcal{N} = 7$ neutrons) (30).

6. FEEDING AND DECAY OF SUPERDEFORMED BANDS

Superdeformed bands are populated to much higher spins than states with smaller deformation (referred to as "normal" states hereafter) and have about an order of magnitude larger intensity than might be expected from the intensity pattern of the normal states (10, 78). These features make it interesting to try to understand the population mechanism. Important elements affecting the feeding are the level densities of both normal and superdeformed states, the mixing between the two classes of states at moderate excitation energy, and the electromagnetic decay rates in the normal and superdeformed minima (78, 79), as well as the barrier separating the two minima (80). Thus, investigations of the feeding mechanism also yield information on these aspects, providing perhaps the main incentive for such studies. Furthermore, knowledge of this mechanism allows selection of optimal conditions (in terms of reaction and bombarding energy) for spectroscopic studies of superdeformation.

Insight on the feeding mechanism may be obtained from data for both superdeformed and normal states on (*a*) population intensities as a function of spin and beam energy for one or several projectile-target combinations; (*b*) distributions in spin and energy at entry into the final nucleus; (*c*) shapes of the quasicontinuum and statistical spectra associated with the feeding of the two classes of states; and (*d*) the properties of ridge structures in E_γ-E_γ correlation matrices. Unfortunately, data on this problem have not kept pace with the steady flow of information on the many superdeformed bands discussed above. Only (*a*) and (*b*) are discussed here. [Moore et al (81) discuss (*c*); Nolan & Twin (10) and Schiffer et al (79) discuss (*d*).]

6.1 *Intensities of Superdeformed Bands*

Figure 12 presents, as a function of the rotational frequency $\hbar\omega$, the relative intensities of transitions in ^{149}Gd and ^{192}Hg, which are representative of superdeformed nuclei in their respective regions. In the $A = 150$ region, the number of coincident γ rays is generally larger and the transition

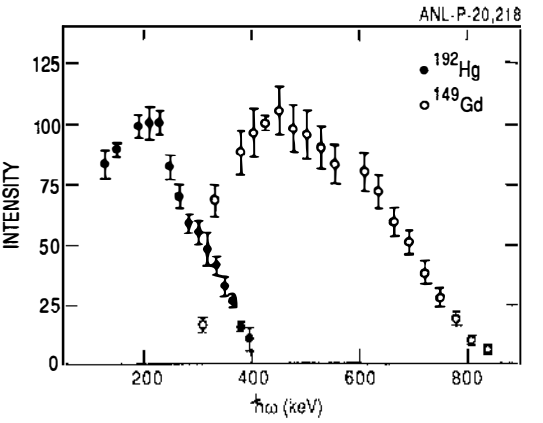

Figure 12 Relative intensities as a function of frequency $\hbar\omega$ for ^{192}Hg (22) and ^{149}Gd (44), normalized to 100 at their respective maxima.

energies are almost twice as large. The larger transition energy is principally due to the larger spins of the emitting states and, to a lesser extent, to the smaller moments of inertia. The first and last transitions in the superdeformed bands in ^{149}Gd and ^{192}Hg correspond to estimated spins of (63/2, 131/2$\hbar$) and (10, 42$\hbar$), respectively (22, 23, 44). In both cases, the population extends to much higher spin than in the normal states. Figure 12 also shows another similarity between bands in the two regions: as the spin decreases, the intensity gradually increases, flattens out at the maximum, and then drops rapidly within a couple of transitions as the bands decay to the lower-lying normal states. The superdeformed bands are weakly populated in all cases, with maximum intensities reaching about 1 and 2% in the $A = 150$ and $A = 190$ regions, respectively.

6.2 *Entry Distributions*

The entry distribution, representing the population distribution in spin and excitation energy after neutron emission, can be measured for superdeformed and normal states with 4π detector calorimetric arrays. Together with Compton-suppressed Ge detectors, these arrays constitute the detection systems used in all superdeformation studies. Data on complete distributions have not been published, but information exists on the average entry points, that is, the centroids of the distributions. The latter have been derived from data on the sum-energy (the total γ-ray energy emitted) and fold (average number of detectors firing) measured in coincidence with discrete normal or superdeformed transitions. The entry points for normal and superdeformed states in ^{192}Hg, measured at several bombarding ener-

gies with the ^{160}Gd(^{36}S,4n) reaction, are shown in Figure 13*a* (80). The entry spins for the superdeformed states are higher than those for the normal states, and the initial population leading to superdeformed states is colder, i.e. the entry points are lower in excitation energy than those of normal states at the same spin. Similar data on entry points for the $A = 150$ region have not been published, but the sum-energy and fold for normal and superdeformed states in ^{149}Gd have been measured (Figure 13*b*) (82). Because spin scales approximately linearly with fold, feeding of superdeformed bands also originates from higher spin and lower energy, as for ^{192}Hg. Thus, feeding of superdeformed bands in both $A = 150$ and $A = 190$ regions share common characteristics.

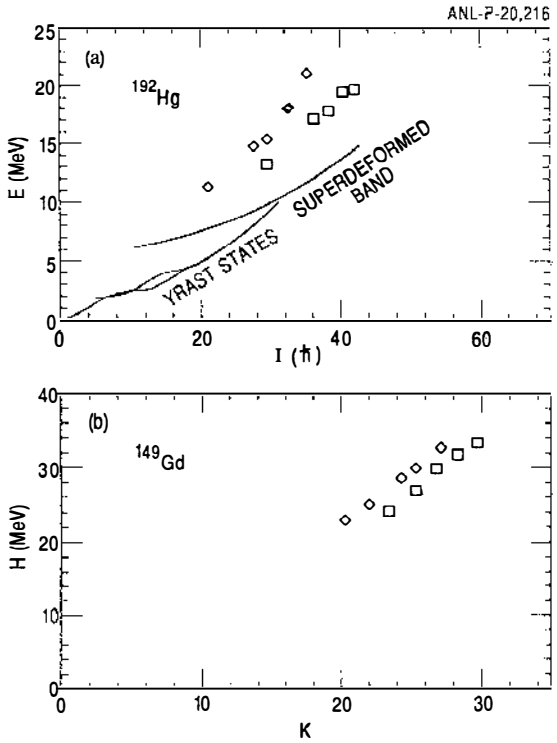

Figure 13 (*a*) Entry points for normal (*diamonds*) and superdeformed (*squares*) states in ^{192}Hg measured in the ^{160}Gd(^{36}S,4n) reaction at several bombarding energies (80). The known yrast states are indicated; the energy of the superdeformed band is not known and is arbitrarily chosen.

(*b*) Average sum-energy H and fold K for normal and superdeformed states in ^{149}Gd measured at a number of projectile energies in the ^{124}Sn(^{30}Si,5n) reaction (82).

Since the entry spins for ^{149}Gd must necessarily be larger than the average spin where the discrete superdeformed band is fed ($\sim 111/2\hbar$), the spins of the states from which the superdeformed bands originate are larger in ^{149}Gd than in ^{192}Hg. On the other hand, the maximum angular momenta brought into the compound nuclei are comparable in the two cases. The lower entry spin in ^{192}Hg is attributed to the depletion of the highest partial waves by fission, which predominates over evaporation residue formation beyond spin $40\hbar$ (80). (Thus, superdeformed bands have been identified in this nucleus near to the limit of fission instability.) It is striking that the feeding of the superdeformed bands originates from the highest spins in the evaporation residues. This occurs because the level densities of superdeformed states exceed those of the normal states only for the highest spins.

Schiffer and Herskind, in an extensive series of calculations, have successfully described many of the observed feeding features in ^{152}Dy and have provided insight into the population mechanism (78, 79). The calculations start by describing the first phase of the decay of the compound nucleus (neutron evaporation and fission) to obtain an entry distribution in spin and energy from which γ decay occurs. The decay is then followed through Monte Carlo simulations and consists of a competition at each step between electromagnetic decay (E1 statistical γ decay, which cools the nucleus, and collective E2 γ decay, which removes two units of angular momentum) in the normal and superdeformed wells, and hopping between the normal and superdeformed wells. As the energy increases, the level density for the superdeformed states increases less rapidly than for the normal states. This results in a limited region in excitation energy in which the density of superdeformed states is larger than that of normal states. This region corresponds to the highest partial waves and is located roughly beyond the point where the superdeformed band crosses the normal states and becomes yrast (Figure 13). Schiffer and Herskind suggest that the entry states for the superdeformed band originate from this region and that this feature accounts for the "colder" feeding of the superdeformed bands. Although the barrier between the superdeformed and normal states was included in the calculations and governed the tunneling between the two wells, its role was not emphasized. The barrier may, in fact, play the pivotal role since mainly entry states within the superdeformed well (states that are below the barrier) are likely to be trapped within the well (80). If this is indeed the case, then the entry energy is closely related to the barrier energy. As a result, a measurement of the entry points could provide a determination of the barrier and also of the superdeformed well depth, although the latter requires knowledge of the excitation energy of the band. These quantities are directly related to the shell correction responsible for

the superdeformed pocket, and thus they are interesting to compare with theoretical values.

6.3 *Deexcitation of Superdeformed Bands*

The sudden decrease of superdeformed transition intensities at low frequencies (Figure 12) indicates that, after a long cascade of consecutive intraband transitions, a rapid decay toward the lower-lying normal states takes place. So far, none of the decay paths linking the superdeformed bands with the normal states has been identified in the $A = 150$ or 190 regions, which suggests that the decay is fragmented into many pathways, each too weak to define, and is probably statistical in nature (78). It has, therefore, not been possible to define the spins and excitation energies of superdeformed band levels with standard spectroscopic techniques. This task remains the major challenge in the study of superdeformation.

The transition from a superdeformed to a normal shape represents a large amplitude motion involving a drastic structural rearrangement. It is perhaps not surprising that the decay is fragmented into many intermediate excited states involving, in some cases, a time delay before the yrast line is reached (21, 83).

The deexcitation of superdeformed bands represents an interesting problem addressed by a number of recent calculations (78, 84, 85). As γ decay occurs within a superdeformed band, a curious situation arises where the excitation energy of the superdeformed states with respect to the yrast levels increases (see Figure 13*a*). At the point of decay, the superdeformed levels have an estimated energy of 3–6 MeV above yrast. Hence, a cold state, isolated within its own potential well, is immersed in a hot sea of normal states with very high density. The decay then occurs through admixtures with this sea of states. Properties of the decay, e.g. the spin dependence of the out-of-band decay probability, can provide information on the mixing between the superdeformed and normal states and on the barrier separating them. The gross energy distribution of the decay γ rays may also provide additional information. (It may be easier to determine this distribution than to trace out the individual pathways.)

7. SUMMARY AND OUTLOOK

Superdeformed nuclei have now been discovered in four distinct regions of the periodic table with masses around $A = 130$, 150, 190, and 240, and with respective axis ratios of 3:2, 1.9:1, 1.7:1, and 2:1. These coincide with the regions where theory, which incorporates a macroscopic liquid-drop term and a quantal shell-correction term, also predicts the occurrence of nuclei with very large deformation. This success represents a triumph

for the Strutinsky method, and for mean-field theories in general, in describing the macroscopic and microscopic aspects of nuclear behavior.

In the $A = 150$ and 190 regions reviewed here, it has been possible to perform spectroscopic studies in the superdeformed secondary well, and both "ground" and excited bands have been observed. An unexpected discovery is that a number of the excited bands have energies identical to those of the lowest superdeformed bands in adjacent nuclei. The degeneracies of better than one part in 500 require that the moments of inertia be identical and also that the strong coupling limit applies, both to a remarkable degree. It is not clear whether this is a result of an accident or is a consequence of a symmetry that has yet to be identified. Perhaps models that exploit symmetries, such as the interacting boson model (86), may shed light on this question. One also wonders if the identical energies of bands in even and odd nuclei might be a manifestation of supersymmetry which covers both fermion and boson degrees of freedom (87). Pseudo-spin alignment partially accounts for identical energies in superdeformed bands of some adjacent even and odd nuclei, but it is not clear if it plays a significant role in other identical bands.

Although there has been much progress in research on superdeformation, many questions remain and, indeed, new questions have been raised by the new discoveries. Certainly, a major challenge is to determine the excitation energies and spins of superdeformed levels since there is not a single superdeformed band in the $A = 150$ and 190 regions for which these properties are known. The borders of the regions of superdeformation in the periodic table need to be established. The known excited superdeformed bands are believed to correspond to particle or quasiparticle excitations, but the collective modes associated with states of large deformation—for example the beta, gamma, or octupole vibrations—are yet to be found. If the deformation is stiff with respect to quadrupole distortion, the beta vibrations may lie at high excitation energies, but soft octupole modes may exist at lower energies (88), possibly giving rise to exotic bending modes. To shed more light on the cause of identical bands, it will probably be necessary to identify higher-lying particle states that can be used, for instance, to search for evidence of pseudo-spin orbit doublets and pseudo-spin alignment, as described in Section 3.4.

Investigations of the mixing between states in the normal and superdeformed well will give information on the barrier separating them and on the superdeformed well depth. Both quantities are important to study because they are direct manifestations of the shell corrections leading to the formation of the superdeformed pocket. Mixing in excited states can be investigated through the properties of ridges in the E_γ-E_γ matrices and, at higher energies, by studying the feeding mechanism of superdeformed

bands. Finally, mixing between cold superdeformed states and excited normal ones can be studied through the decay properties involved in the deexcitation out of superdeformed bands.

At present, experiments are limited by the detection capabilities of current γ-ray detectors. The next generation of detector arrays currently under construction (GAMMASPHERE in the United States and EUROGAM in Europe) will improve the detection sensitivity by about two orders of magnitude and provide answers to the questions raised above. Many fascinating discoveries about superdeformation—and about nuclear structure in general—lie ahead.

ACKNOWLEDGEMENTS

The data and ideas reviewed above are the result of dedicated work by many colleagues and friends. It is impossible to name them all here. We would like, however, to acknowledge the contributions of our collaborators at Argonne, Notre Dame, Purdue, I.N.E.L., Stockholm, and Warsaw. We also thank Mike Carpenter, Patricia Fernandez, and Frank Moore for carefully reading the manuscript. This work was supported by the Department of Energy, Nuclear Physics Division, under contract number W-31-109-ENG-38.

Literature Cited

1. Strutinsky, V. M., *Nucl. Phys.* A95: 420–42 (1967); A122: 1–33 (1968)
2. Polikanov, S. M., et al., *Sov. Phys. JETP* 15: 1016–21 (1962)
3. Tsang, C. F., Nilsson, S. G., *Nucl. Phys.* A140: 275–88 (1970)
4. Bengtsson, R., et al., *Phys. Lett.* B57: 301–5 (1975)
5. Ragnarsson, I., et al., *Nucl. Phys.* A347: 287–315 (1980)
6. Dudek, J., Nazarewicz, W., *Phys. Rev.* C31: 298–301 (1985)
7. Chasman R. R., *Phys. Lett.* B187: 219–23 (1987)
8. Twin, P. J., et al., *Phys. Rev. Lett.* 57: 811–14 (1985)
9. Kirwan, A. J., et al., *Phys. Rev. Lett.* 58: 467–70 (1987)
10. Nolan, P. J., Twin, P. J., *Annu. Rev. Nucl. Part. Sci.* 38: 533–62 (1988)
11. Bohr, A., Mottelson, B. R., *Nuclear Structure*, Vol. 2. Reading, Mass: Benjamin (1975)
12. Nilsson, S. G., et al., *Nucl. Phys.* A131: 1–66 (1969)
13. Åberg, S., *Phys. Scr.* 25: 23–27 (1982)
14. Bengtsson, T., Ragnarsson I., *Nucl. Phys.* A436: 14–82 (1985)
15. Chasman, R. R., *Phys. Lett.* B219: 227–31 (1989)
16. Girod M., et al., *Phys. Rev. Lett.* 62: 2452–56 (1989)
17. Bonche, P., et al., *Nucl. Phys.* A500: 308–22 (1989)
18. Moore, E. F., et al., *Phys. Rev. Lett.* 63: 360–63 (1989)
19. Nazarewicz, W., et al., *Phys. Lett.* B225: 208–14 (1989)
20. Bengtsson, T., et al., *Phys. Lett.* B208: 39–43 (1988)
21. Riley, M. A., et al., *Nucl. Phys.* A512: 178–88 (1990)
22. Ye, D., et al., *Phys. Rev.* C41: R13–16 (1990)
23. Becker, J. A., et al., *Phys. Rev.* C41: R9–12 (1990)

24. Hubel, H., et al., *Nucl. Phys.* A453: 316–48 (1986)
25. Moore, E. F., et al., *Phys. Rev. Lett.* 64: 3127–30 (1990)
26. Nazarewicz, W., et al., *Nucl. Phys.* A503: 285–330 (1989)
27. Bengtsson T., et al., *Nucl. Phys.* A496: 56–65 (1989)
28. Carpenter M. P., et al., *Phys. Lett.* B240:44–49 (1990)
29. Janssens, R. V. F., et al., *Nucl. Phys.* A520: 75c–90c (1990)
30. Drigert, M. W., et al., et al., *Nucl. Phys.* A530: 452–74 (1991)
31. Henry E. A., et al., *Z. Phys.* A335: 361–62 (1990)
32. Cullen, C. M., et al., *Phys. Rev. Lett.* 65: 1547–50 (1990)
33. Beausang, C. W., et al., *Z. Phys.* A335: 325–30 (1990)
34. Fernandez, P. B., et al. *Nucl. Phys.* A517: 386–98 (1990)
35. Azaiez, F., et al., *Z. Phys.* A336: 243–44 (1990); *Phys. Rev. Lett.* 66: 1030–33 (1991)
36. Brinkman, M. J. et al., *Z. Phys.* A336:115–16 (1990)
37. Theine, K., et al., *Z. Phys.* A336: 113–14 (1990)
38. Nazarewicz, W., In *Proc. XXV Zakopane Sch. on Physics*, to be published (1991)
39. Chasman, R. R., *Phys. Lett.* B242: 317–22 (1990)
40. Stephens, F. S., et al., *Phys. Rev. Lett.* 64:2623–26 (1990); 65: 301–4 (1990)
41. Hebbinghaus, G., et al., *Phys. Lett.* B240: 311–16 (1990)
42. Zuber, K., et al., *Nucl. Phys.* A520: 195c–200c (1990); *Phys. Lett.* B254: 308–14 (1991)
43. Deleplanque, M. A., et al., *Phys. Rev. Lett.* 60:1626–29 (1988)
44. Haas, B., et al., *Phys. Rev. Lett.* 60: 503–6 (1988); *Phys. Rev.* C42: R1817–21 (1990)
45. Fallon, P., et al., *Phys. Lett.* B218: 137–42 (1989); B257: 269–72 (1991)
46. Janzen, V. P., et al., In *Proc. Int. Conf. on High Spin Physics and Gamma-soft Nuclei.* Pittsburgh: World Scientific (1991), pp. 225–43
47. Deleplanque, M. A., et al., *Phys. Rev.* C39: 1651–54 (1989)
48. Rathke, G.-E., et al., *Phys. Lett.* B209: 177–81 (1988)
49. Johansson, J. K., et al., *Phys. Rev. Lett.* 63: 2200–3 (1989)
50. Lieder, R. M., et al., *Nucl. Phys.* A520: 59c–66c (1990)
51. Twin, P. J., *Nucl. Phys.* A520: 17c–33c (1990); Mullins S. M., et al., *Phys. Rev. Lett.* 66: 1677–80 (1991)
52. Shimizu, Y. R., et al., *Phys. Lett.* 198B: 33–38 (1989); *Nucl. Phys.* A509: 80–116 (1990)
53. Byrsky, T., et al., *Phys. Rev. Lett.* 64: 1650–53 (1990)
54. Nazarewicz, W., et al., *Phys. Rev. Lett.* 64: 1654–58 (1990)
55. Twin, P. J., *Nucl. Phys.* A522: 13c–30c (1991)
56. Hecht, K. T., Adler, A., *Nucl. Phys.* A137: 129–43 (1969)
57. Arima, A., et al., *Phys. Lett.* B30: 517–22 (1969)
58. Ratna-Raju R. D., et al., *Nucl. Phys.* A202: 433–66 (1973)
59. Bohr, A., et al., *Phys. Scr.* 26: 267–72 (1982)
60. Mottelson, B., *Nucl. Phys.* A520: 711c–22c (1990)
61. Deleted in proof
62. Ragnarsson, I., *Nucl. Phys.* A520: 67c–74c (1990)
63. Stephens, F. S., *Nucl. Phys.* A520: 91c–104c (1990)
64. Satula, W., et al., *Nucl. Phys.* In press (1991)
65. Becker, J. A., et al., *Nucl. Phys.* A520: 188c–94c (1990)
66. Draper, J. E., et al., *Phys. Rev.* C42: R1791–95 (1990)
67. Wu, C., et al., *Phys. Rev. Lett.* 66: 1377–78 (1991)
68. Wyss, R., Pilotte, S., *Phys. Rev. C.* In press (1991)
69. Harris, S. M., *Phys. Rev.* B509: 138–54 (1965)
70. Carpenter, M. P., et al., to be published (1991)
71. Nazarewicz, W., *Nucl. Phys.* A520: 333c–51c (1990) and references therein
72. Höller, J., Åberg, S., *Z. Phys.* A336: 363–64 (1990)
73. Åberg, S., *Nucl. Phys.* A520: 35c–57c (1990)
74. Dudek, J. et al., *Phys. Lett.* 248B: 235–42 (1990)
75. Bonche, P. et al., *Phys. Rev. Lett.* 66: 876–79 (1991)
76. Szymanski, Z., *Nucl. Phys.* A520: 1c–16c (1990)
77. Wyss, R., Johnson, A., see Ref. 46, pp. 123–32
78. Herskind, B., Schiffer, K., *Phys. Rev. Lett.* 59: 2416–19 (1987)
79. Schiffer, K., et al., *Z. Phys.* A332: 17–27 (1989)
80. Khoo, T. L., et al., *Nucl. Phys.* A520: 169c–77c (1990)
81. Moore, E. F., et al., In *Proc. Workshop on Nuclear Structure and Heavy-ion Reaction Dynamics, Inst. Phys. Conf. Ser.* 109: 171–78 (1991)
82. Taras, P. et al., *Phys. Rev. Lett.* 61:

1348–51 (1988); Haas, B., et al., *Phys. Lett.* B245: 13–16 (1990)
83. Carpenter, M. P., et al., *Nucl. Phys.* A520: 133c–37c (1990)
84. Vigezzi, E., et al., *Phys. Lett.* B249: 163–67 (1990)
85. Bonche, P., et al., *Nucl. Phys.* A519: 509–20 (1990)
86. Iachello, F., Arima, A., *The Interacting Boson Model.* Cambridge Univ. Press (1987); Iachello, F., *Nucl. Phys.* A522: 83c–98c (1991)
87. Iachello, F., van Isacker, P., *The Interacting Boson Fermion Model*, Cambridge Univ. Press (1990)
88. Mizutori, S., et al., to be published (1991)